Enhanced low-frequency microwave absorption performance of FeNi alloy coated carbon foam assisted by SiO2 layer

Yangjun Zou, Xiaozhong Huang, Benhui Fan, Jianling Yue, Yu Liu

Enhanced low-frequency microwave absorption performance of FeNi alloy coated carbon foam assisted by SiO_2 layer

Yangjun Zou[1,2], Xiaozhong Huang[1,2], Benhui Fan[3], Jianling Yue[1,2]*, Yu Liu[1,2]*

1 State Key Laboratory of Powder Metallurgy, Powder Metallurgy Research Institute, Central South University, 410083 Changsha, PR China

2 Hunan Key Laboratory of Advanced Fibers and Composites, Central South University, Changsha, Hunan 410083, PR China

3 Cerema, Research Team ENDSUM, 23 avenue de l'Amiral Chauvin, 49136 Les Ponts de Cé, France

Corresponding author: Y. Liu (yu_liu@csu.edu.cn), J. Yue (jlyue2010@csu.edu.cn);

Abstract:

The hierarchical structures of carbonized melamine foam modified by FeNi alloy and silicon layer (CMF/FeNi-SiO_2) have been fabricated by a magnetron sputtering method. The as-prepared CMF/FeNi-SiO_2 composites exhibited a three-dimensional porous structure, with the framework uniformly covered by a 150~400 nm FeNi layer and an ultrathin SiO_2 layer, which demonstrated soft magnetic properties at room temperature. Moreover, the microwave absorption performance of the foam was investigated in the frequency range from 2 to 18 GHz. The results showed that the microwave absorption performance of CMF/FeNi-SiO_2 composite was significantly enhanced in the low-frequency range compared with CMF/FeNi. The minimum reflection loss of CMF/FeNi-SiO_2 with an absorption thickness of 4.1 mm was about −53 dB at 3.38 GHz and reached an effective absorption bandwidth of 0.93 GHz (from 2.93 GHz to 3.86 GHz). The frequency bandwidth of 4 GHz (2.35~6.35 GHz) with absorption loss ≤ −10 dB and the frequency bandwidth of 2.05 GHz (2.62~4.67

GHz) with absorption loss ≤ -20 dB demonstrated the CMF/FeNi-SiO_2 a high-efficient absorber in the low-frequency band (2-6 GHz), which stemmed from improved impedance matching and attenuation capacities.

Keywords: Carbon foam, FeNi alloy, SiO_2 layer, Low-frequency electromagnetic microwave absorption

1 Introduction

With the great progress in science and technology, electronic instruments and communication technologies have brought great convenience to human life[1]. However, various electromagnetic pollution has emerged simultaneously due to the wave's radiation that not only potentially threatens human health but also leads to the interference of communications[2, 3]. Therefore, the development of effective electromagnetic microwave (EMW) absorbing materials is an urgent requirement to solve these problems.

Generally, an ideal absorption material is usually expected to have low density, thin thickness, and strong EMW absorption ability within a wide frequency bandwidth [4]. Generally speaking, microwave absorption materials can be classified as carbon materials[5, 6], ferrite materials[7-9], magnetic alloy[10-13], ceramic materials[14-17], and other kinds of materials[4, 18-21]. Among them, carbon-based materials are favored by more and more researchers thanks to their outstanding properties, such as stable physicochemical properties, lightweight, easy accessibility, low price, high processibility, etc.[6, 22, 23].

Carbon foam, carbonized from melamine foam (CMF), is a typical lightweight material, which integrates conventional dielectric absorbing carbon materials and porous structures. Due to its excellent electromagnetic properties such as interface polarization, porous scattering and diffraction, and good thermal stability, carbon

foam has attracted much attention[6, 24-27]. Many works have been reported around the application of CMF in EMW shielding and absorption. For instance, Ye et al. prepared a SiC coating/porous carbon foam composite by using carbonization and chemical vapor deposition route. The obtained sample could achieve a minimal RL of -25.93 dB at 17.2 GHz with a thin thickness of 1.05 mm[28].

Although the structural advantages of CMF make it a candidate for microwave absorbers, there are still some unavoidable drawbacks limiting its further applications. One big disadvantage is that the rich amount of nitrogen from melamine in carbon foam can alter the distribution of valent electron clouds in carbon chains resulting in the relatively high conductivity[29]. Thus, when the incident waves arrive on the surface of C foam, most of them will be reflected directly, which means much more shielding than absorption[30]. Even though a small amount of EMW enteres C foam, as a diamagnetic material, the impedance mismatch caused by the low magnetic permeability and high conductivity would also reduce the absorption performance. In this case, based on the absorption mechanism, the combination of carbon foam with magnetic materials can effectively improve the magnetic loss of carbon foam to help the absorption of EMW[31]. Qiu et al. fabricated porous cobalt iron alloys and carbon (CoFe@C) composites, the optimal reflection loss of CoFe@C submicrocubes with mesoporous structure was −73.63 dB at 2.6 mm, and the effective absorption bandwidth (EAB, reflection loss (RL) ≤ -10 dB) reached 5.0 GHz[32]. Yin et al. obtained a composite of unique biconical carbon framework decorated with $CoFe_2O_4$ and (Fe,Ni) nanoparticles, which owned minimal RL of −34.3 dB at 12.92 GHz for 2.0 mm with its broadest EAB of 6.55 GHz at only 1.87 mm, showing excellent dielectric loss capacity for microwave absorption[33].

However, the dielectric constant of magnetic film is much larger than its

magnetic permeability, leading to a strongly reflective performance. On the other hand, metal magnetic films tend to have a large electrical conductivity, and the influence of the skin effect on microwave penetration and absorption causes strong reflection. Therefore, it is necessary to reduce the dielectric constant of the film to match the dielectric constant and permeability, and the resonance penetration will be beneficial to the absorption of low-frequency microwaves.

To solve this problem, coating a certain insulating layer on the magnetic metal can not only reduce the electrical conductivity of the systems for preferable impedance matching but also help reduce the energy loss caused by the eddy current effect [35-37]. A potential insulating material for this application is SiO_2. As an excellent dielectric material, it has high resistivity (~$10^{16}\,\Omega\cdot$cm) and helps to improve the impedance matching of carbon material, thus reducing electromagnetic waves reflection.[38-40] In addition, coating SiO_2 on the magnetic metal surface will not inhibit the permeability. Michael Green et al. reported one doped SiO_2 nanoparticle with an RL_{min} of -55.09 dB because of the electrical relaxation[41]. Therefore, the combination of magnetic metal and SiO_2 in the carbon foam system can be a possible solution to improve EMW absorption.

In this study, a facile magnetron sputtering method was employed to deposit a double-layer film on the carbon foam for the preparation of hybrid CMF/FeNi-SiO_2 foam, where the inner layer was magnetic FeNi alloy, and the outer layer was SiO_2 insulating layer. By analyzing the microstructural properties including layer's morphology, foam's three-dimensional structure, and the magnetic properties of the samples, the synthetical effects of the microstructures, magnetic properties, and impedance matching on the EMW absorption were systematically discussed and studied in the following parts.

2 Experimental

2.1 Materials and preparation

Melamine foam (MF) was manufactured by Beijing Kelinmei High-Tech Materials co., LTD. Ferronickel target ($Fe_{50}Ni_{50}$, purity > 99.99%) and silicon oxide target clips (SiO_2, purity > 99.99%) were purchased from Zhangzhou Heqi target Technology Co., Ltd. Tetraethyl orthosilicate (TEOS) and ammonia solution ($NH_3 \cdot H_2O$) were provided by Sinopharm Chemical Reagent Co., Ltd. MF was carbonized at 800 °C for 6h under Argon atmosphere to obtain the carbon foam, named as CMF.

Magnetron sputtering method was applied to coat FeNi alloy on the CMF. The base pressure was about 6.0×10^{-4} Pa, and the argon pressure was maintained at 0.3 Pa. Firstly, a layer of FeNi alloy film was sedimented on the CMF by direct current (DC) magnetron sputtering with a fixed current of 4 A for 10 min and 15 min for each side, named as CMF/FeNi10 and CMF/FeNi15, respectively. Then, SiO_2 films were coated on the CMF/FeNi by radio frequency (RF) magnetron sputtering under power at 800 W for 2 h on each side. The prepared samples were named as CMF/FeNi10-SiO_2 and CMF/FeNi15-SiO_2, individually. The fabrication process of CMF/FeNi-SiO_2 hybrids is illustrated in Figure 1.

As a comparison, CMF/FeNi10 was modified with more SiO_2 by a liquid phase method[42]. Firstly, CMF/FeNi10 was put into a 1 L beaker with distilled water (100 mL) and ethanol (400 mL). After magnetic stirring for 1 h, 7 ml ammonium hydroxide was added to adjust the pH to 9.0. Secondly, a thick layer of SiO_2 was loaded on the surface of the CMF/FeNi10 by the hydrolysis of 3 ml TEOS in a basic solution. After magnetic stirring overnight at room temperature, the foam was removed from the solution and dried in a vacuum oven at 60°C for 4 h. The obtained

sample was named as CMF/FeNi10-SiO_2(L).

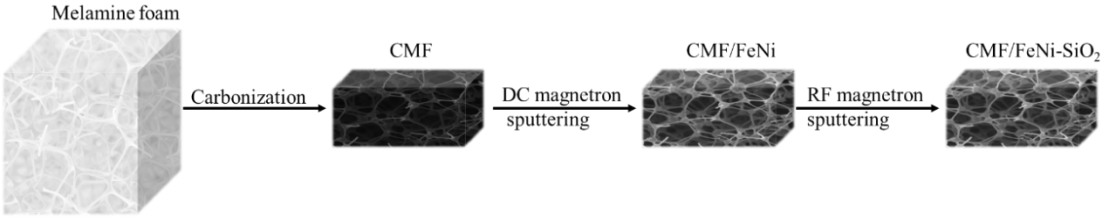

Figure 1 Diagram of the fabrication of the CMF/FeNi-SiO_2 hybrids

2.2. Characterization

A scanning electron microscope (SEM, TESCAN MIRA3 LMU), equipped with energy dispersive spectroscopy (EDS), was used to investigate the microstructure of these samples. To study the crystal structures of the CMF materials, an X-ray diffractometer (XRD, PANalytical Empyrean) were applied to obtain X-ray diffraction patterns. The chemical structure of the material surface was analyzed by X-ray photoelectron spectroscopy (XPS) with an AXIS SUPRA+ system. Vibrating sample magnetometers (VSM, Lake Shore7404) were used to detect the hysteresis loops of samples. The carbon contents were evaluated by thermogravimetric analysis (TGA, Netzsch TG 209F1 Libra) in the air at a temperature range of 25 to 800 °C with a heating rate of 10 °C/min. Lastly, analysis of the electromagnetic parameters of the foams in the frequency range from 2 to 18 GHz was performed using a vector network analyzer (8720ET, Agilent) by a coaxial method. The foams were impregnated in resin and then cut into coaxial rings with an outer diameter of 7.0 mm, an inner diameter of 3.04 mm, and a thickness of 2 mm. The reflection loss (RL) was calculated by the following formulas[43]:

$$RL = 20log_{10}\left|\frac{Z_{in}-Z_0}{Z_{in}+Z_0}\right| \quad (1)$$

$$Z_{in} = Z_0\sqrt{\frac{\mu_r}{\varepsilon_r}}tanh\left[j\left(\frac{2\pi fd}{c}\right)\sqrt{\mu_r\varepsilon_r}\right] \quad (2)$$

$$Z_0 = \sqrt{\frac{\mu_0}{\varepsilon_0}} \quad (3)$$

Where Z_0, Z_{in}, d, f and c are the impedance value of the air, the input impedance of the absorber, the thickness of the absorber, the given microwave frequency and the speed of light in free space. ε_r and μ_r are the relative permittivity and permeability, respectively.

3 Results and discussion

Figure 2 showed the micromorphology when the CMF was deposited by FeNi with different sputtering times. As shown in Figure 2(a), the CMF remained the three-dimensional porous structure of melamine foam. There were many spheroids of approximately 10 μm diameter at the intersections of skeletons after the carbonatization treatment of melamine foam. This partly structural inflation was caused by the escape of ammonia during the carbonization of melamine foam. After DC magnetron sputtering as indicated in Figure 2(b) and (c), a continuous dense FeNi alloy layer could be observed on the surface of CMF. The corresponding element mapping of CMF/FeNi10 was shown in Figure 2(d) ~ (f), manifesting the uniform distribution of the Fe element and Ni element around the carbon skeleton. The energy dispersive spectrum analysis (EDS, seen in Figure S1) of the CMF/FeNi10 showed the foam was composed of 44.59 wt% C, 19.68 wt% Fe and 22.48 wt% Ni, indicating the FeNi alloy was successfully coated on the carbon foam by a facile magnetron sputtering method.

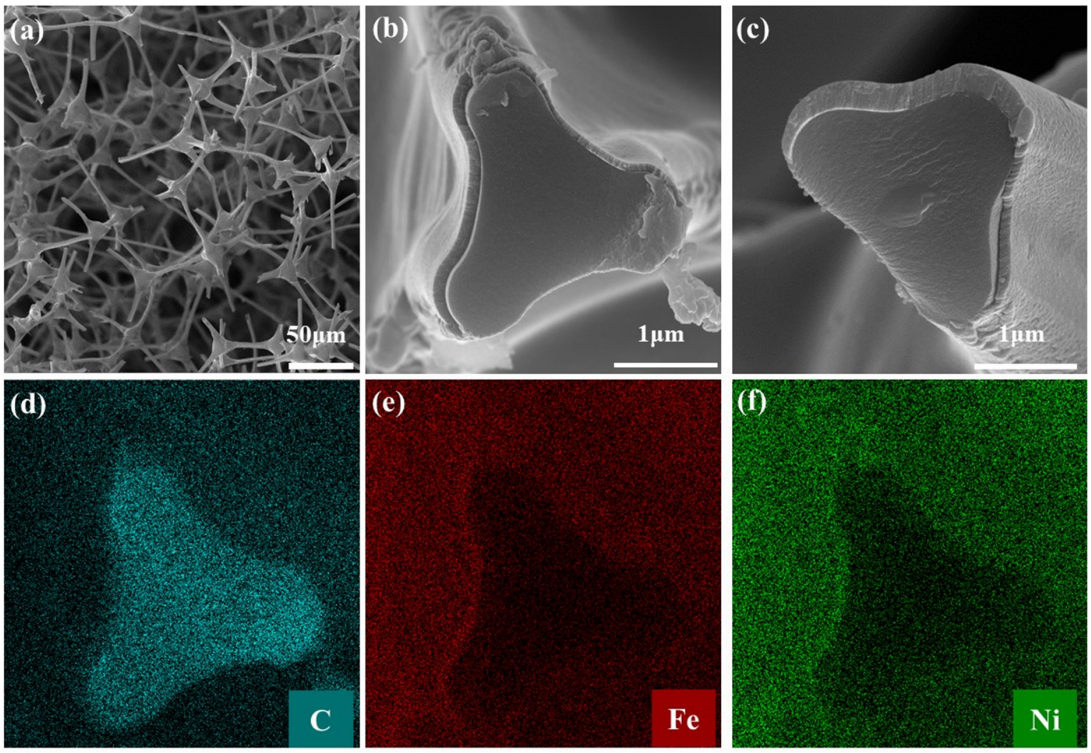

Figure 2 SEM images of (a) CMF, (b) CMF/FeNi10, (c) CMF/FeNi15 and (d) C, (e) Fe and (f) Ni element EDS mapping of CMF/FeNi10.

Figure 3 showed the SEM images of CMF/FeNi15-SiO_2. It can be found that after depositing with SiO_2, the surface of the carbon foam had an obvious double-layer coating, with an inner layer of about 500 nm and an outer layer of about 100 nm. The element mapping images in Figure 3(d) ~ (h) showed that the inner layer was composed of Fe and Ni element while the outer layer was evenly distributed with Si and O element. In addition, the EDS analysis results (in Figure 3(i)) showed that the Si contents of the inner and outer layers were 0.31 wt% and 5.91 wt%, respectively, again proving that the carbon foam was covered by FeNi-SiO_2 bilayers. The above results suggested that the FeNi alloy and SiO_2 were both successfully coated on the foam by magnetic sputtering and the layer contents could be easily controlled by changing the sputtering duration. As a comparison, the SEM images of the CMF/FeNi10-SiO_2(L) synthesized by the liquid phase method was shown in

Figure S2. From Figure S2, it can be seen that the carbon sphere was coated by a continuous FeNi alloy layer and a dense SiO_2 layer. The SiO_2 layer was consisted of many nanospheres with diameters of about 400 nm that were closely connected. EDS energy spectrum showed that the produced foam had 14.47 wt% Si and 15.18 wt% O, which was much higher than the content of CMF/FeNi15-SiO_2 with the value of 5.91 wt% Si and 2.46 wt% O prepared by magnetron sputtering.

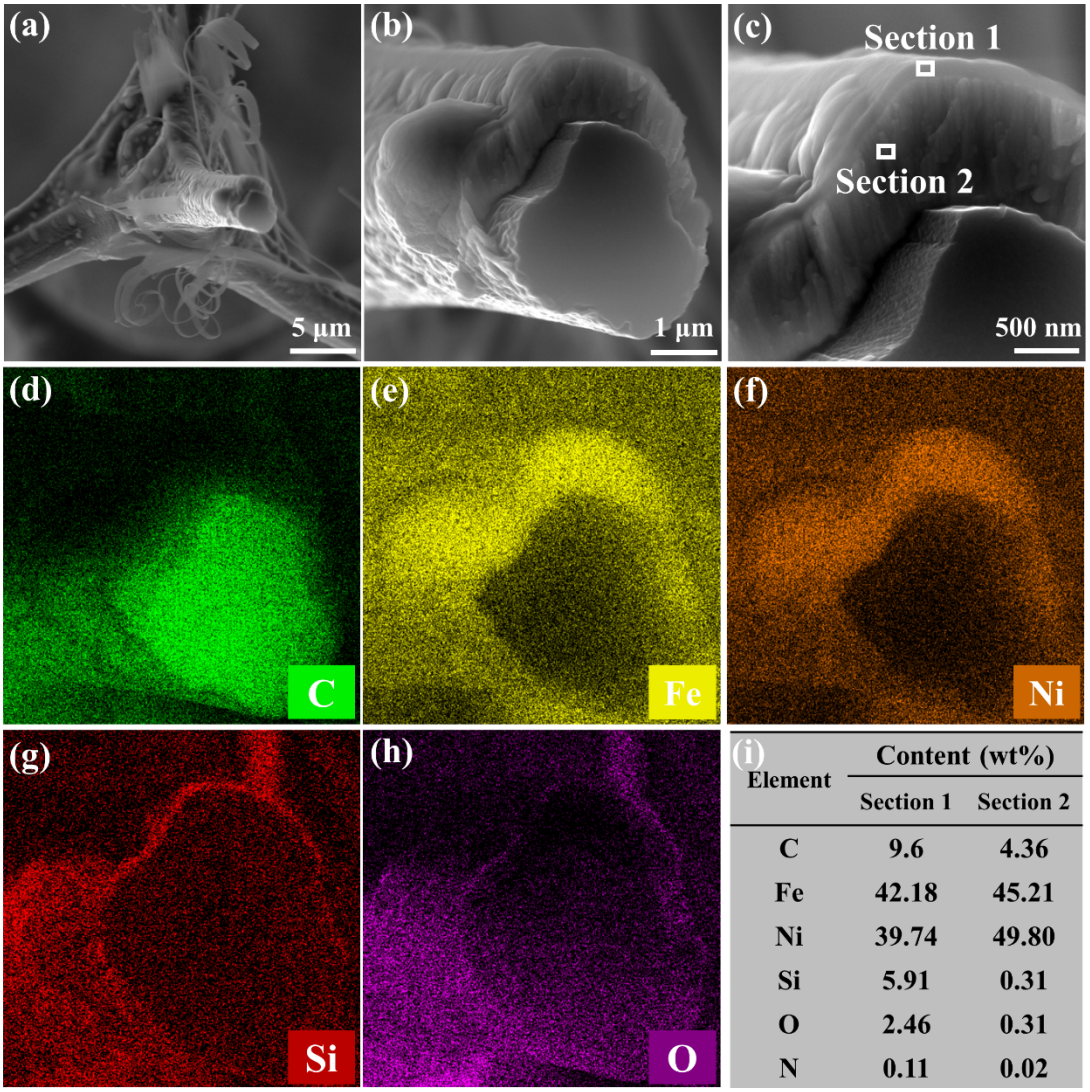

(i)

Element	Content (wt%)	
	Section 1	Section 2
C	9.6	4.36
Fe	42.18	45.21
Ni	39.74	49.80
Si	5.91	0.31
O	2.46	0.31
N	0.11	0.02

Figure 3 (a) ~ (c) SEM images of CMF/FeNi15-SiO_2, (b) ~ (h) corresponding element mapping of CMF/FeNi15-SiO_2 and (i) EDS analysis of the CMF/FeNi15-SiO_2

The phase structures of the foams were studied by XRD (Figure 4(a)). For CMF, the broad diffraction peak at about 24.8° was attributed to the (002) plane of

graphite carbon (JCPDS No.41-1487), indicating that after high-temperature calcination, the melamine foam was completely converted into graphite carbon in Ar atmosphere. After magnetron sputtering, the FeNi alloy-coated and FeNi-SiO_2 double-coated foams all retained the peaks of graphite carbon in the XRD patterns but there emerged one sharp diffraction peak at 43.74°, which was ascribed to be the (111) crystal planes of FeNi alloy, which was consistent with the PDF standard card JCPDS No.47-1417, proving the FeNi alloy was successfully introduced onto the CMF. However, after magnetron sputtering with SiO_2, compared with CMF/FeNi, the intensity of FeNi characteristic peak in CMF/FeNi-SiO_2 slightly decreased, since the crystal growth of FeNi alloy was limited by SiO_2. In addition, there was no obvious SiO_2 diffraction peak in the patterns since it was in an amorphous form. These results indicated that FeNi - SiO_2 double layers were successfully loaded on carbon foam.

The surface properties of CMF/FeNi10-SiO_2 were further studied by XPS, as shown in Figure 4(b)~(e). Main peaks appeared at 284.8 eV, 102.4 eV, 531.4 eV, 711.4 eV and 856.4 eV in Figure 4(b), proving the presence of C, Si, O, Fe and Ni elements. In Figure 4(c), the spectra of Fe2p of CMF/FeNi10-SiO_2 were deconvoluted into five peaks at ~710.8, ~712.7, ~717.7, ~724.1 and ~726.8 eV, suggesting the attendance of Fe^{2+} and Fe^{3+}. There were four peaks at ~855.8, ~861.7, ~873.6 and ~879.9 eV in the Ni2p spectrum, which can be assigned to the Ni^{2+} and satellite feature [44]. The binding energy peaks of 531.4 eV and 99.5 eV, ascribing to the O_{1s} spectrum and Si_{2p} spectrum, respectively, confirmed the existence of SiO_2 again.

The TGA curves corresponding to the mass changes of foam in the air atmosphere from 25 °C to 800 °C were shown in Figure 4(f). A whole 81.86% mass loss in the temperature range of 25 °C to 800 °C was observed for CMF. The weight loss of carbon foam during the heating process mainly came from low molecular

weight gasses produced and released by carbon combustion, such as CO_2 and CO. The foam composite samples loaded with FeNi alloy showed a slight mass increase at the temperature of 400 °C which was due to the oxidation of the FeNi alloy coating. At 800 °C, the mass loss of CMF/FeNi10 was 54.44%, while the mass loss of the CMF/FeNi15 was 51.47%. More residual weight of CMF/FeNi15 proved that the FeNi content in CMF/FeNi15 was higher than that of CMF/FeNi10, indicating that the extension of sputtering time can effectively control the alloy coating content. During the TGA process, Fe and Ni were oxidized to FeO and NiO, respectively. The Fe and Ni contents in CMF/FeNi10 were 35.44 and 35.8 wt%, respectively. While the Fe and Ni contents in CMF/FeNi15 were 37.75 wt% and 38.13 wt%, respectively, which were similar to the EDS result in Figure 3(i) and slightly higher than those in CMF/FeNi10. After the deposition of SiO_2, a notable residual mass increase was observed for CMF/ FeNi-SiO_2, which was caused by the introduction of SiO_2. According to Figure 4(f), the SiO_2 content of CMF/ FeNi10-SiO_2 and CMF/ FeNi15-SiO_2 was 2.67wt % and 2.26wt %, respectively.

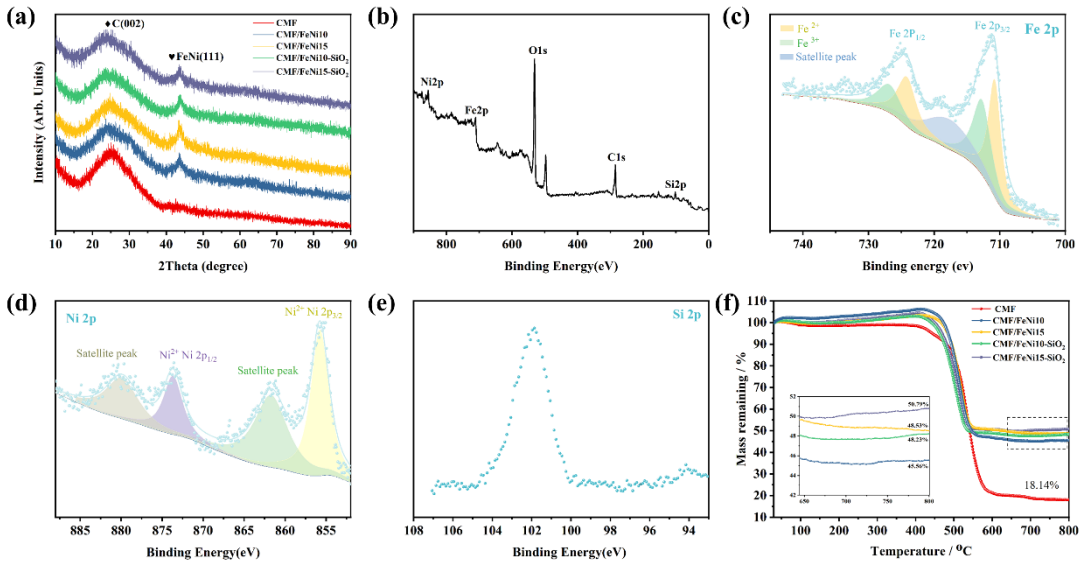

Figure 4 (a) XRD patterns of the CMF-based foams, (b)~(e) XPS survey spectra of

the CMF/FeNi10-SiO_2 and (e) TG curves of foam measured under air condition.

The magnetic properties of CMF/FeNi foam and CMF/FeNi-SiO_2 foam had a great impact on their microwave absorption performance, so the VSM was used to test the magnetic properties of the samples with the magnetic field range of 30000 Oe. Under external magnetic fields, their hysteresis loops were symmetrical closed curves that exhibited typical soft magnetic characteristics. The hysteresis loop was shown in Figure 5. As presented in the curve of CMF/FeNi10 foam, the coercivity (*H*c) value was 55 Oe and the saturation magnetization (*M*s) value was 7.02 emu g^{-1}. As the contents of FeNi increased, both the values of Ms and *H*c raised at the same time. From the inset picture of Figure 5(b), the values of saturation magnetization and coercivity of the CMF/FeNi15 were 8.25 emu g^{-1} and 35 Oe, respectively. The increase of saturation magnetization indicated the higher content of FeNi alloy in CMF/FeNi15. From Figure 5(a), it could be found that the values of saturation magnetization decreased after the deposit of SiO_2 onto FeNi films with 5.37 emu g^{-1} for CMF/FeNi10-SiO_2 and 7.23 emu g^{-1} for CMF/FeNi15-SiO_2, respectively. In spite, the values of coercivity increased after the deposit of SiO_2 with 87 Oe for CMF/FeNi10-SiO_2 and 54 Oe for CMF/FeNi15-SiO_2, respectively. The decline of magnetism was mainly caused by the restricted growth of FeNi crystallites in CMF/FeNi-SiO_2 due to the covered SiO_2.

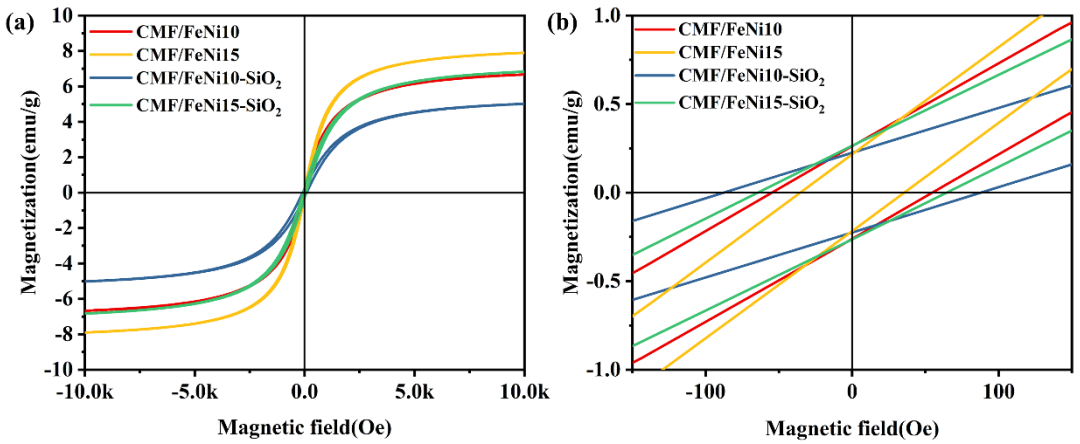

Figure 5 Hysteresis loops for the samples, (a) the magnetic field range was 30000Oe, (b) the magnetic field range was 150Oe.

Figure 6 displayed the three-dimensional reflection loss of the samples at 2~18 GHz at the thickness range of 1 ~ 5 mm, respectively. In Figure 6(a), pristine CMF exhibited limited EMW absorption properties, i.e., the minimum RL with a thickness of 4.3 mm was only -16.8 dB at 10.46 GHz. After being covered by a magnetic FeNi film sputtered for 10min, the EMW absorption performance was improved greatly, with the strongest RL value of -46.64 dB at 9.71 GHz when the thickness was 2.1 mm, as seen in Figure 6(b). With the extension of sputtering time to 15 min, the EMW absorption characteristics of CMF/FeNi15 were further enhanced with an RL_{min} of -54.86 dB at 6.85 GHz at the thickness of 2.7 mm. Although the deposition of a magnetic film on a carbon foam skeleton improved the absorption properties, it was still difficult to meet the general commercial requirements. The absorption capacity of EMW was further enhanced by coating a SiO_2 film on the surface of FeNi film. Notice that the absorption peaks of CMF/FeNi-SiO_2 absorbers in Figure 6(d) and (e) shifted to S and C bands at lower frequencies compared to CMF and CMF/FeNi. When the thickness was 4.3mm, the CMF/FeNi10-SiO_2 achieved an RL_{min} value of -48.26 dB at 4 GHz, and the EAB was 1.33 GHz from 3.47 to 4.78 GHz, corresponding to S and C

bands. Similarly, the RL_{min} value of CMF/FeNi15-SiO_2 was -53 dB at 3.38 GHz, the matching thickness was 4.1mm, and the EAB was located in a lower frequency range from 2.93 to 3.86 GHz. In general, low-frequency microwave absorption has always been the major problem of electromagnetic wave absorption[45]. Interestingly, CMF/FeNi-SiO_2 had strong electromagnetic wave absorption characteristics in the S-band, which meant it had great potential in low-frequency microwave absorption.

To observe the influence of the SiO_2 layer on low-frequency microwave absorption, a detailed analysis of microwave absorption performance was carried out, as shown in Figure 6(f) ~ (i). Notably, the CMF/FeNi15-SiO_2 magnetic and insulating double-layer structure showed the best microwave absorption abilities at 2~4 GHz in Figure 6(h). For example, when the thickness was 4 mm, the RL_{min} values of CMF and CMF/FeNi15 were -14.2 and - 13.8 dB, respectively, as shown in Figure 6(f) and (g). While CMF/FeNi15-SiO_2 exhibited an RL_{min} of -51.8dB at 3.4GHz with an EAB of 1 GHz covering 3 ~ 4 GHz. Besides, the CMF/FeNi15-SiO_2 showed an RL_{min} of -49.3dB and -44dB at 4.5mm and 5mm, respectively, as shown in Figure 6(h). Importantly, the effective absorption bandwidth (RL ≤ -10dB) of CMF/FeNi15-SiO_2 covered 2.35 ~ 6.35 GHz (S ~ C band) with a thickness of 2.4~ 5 mm (in Figure 6(i)). The 2D RL plots of CMF/FeNi10 and CMF/FeNi10-SiO_2 shown in Figure S3 also showed that the introduction of silicon oxide shifted the absorption peak to lower frequencies.To demonstrate the effect of SiO_2 on the low-frequency absorbing properties of CMF/FeNi foams, the reflection loss of CMF/FeNi10-SiO_2(L) with higher SiO_2 content was shown in Figure S4. The microwave absorption properties showed that the CMF/FeNi10-SiO_2(L) had dual-region microwave absorption characteristics, with two strong reflection loss peaks located at 12.3 GHz and 4.13 GHz, and the reflection loss were -55.96 dB and -40.4 dB, respectively. The effective

absorption bandwidth was as wide as 9.86 GHz (3.4~4.6 GHz, 9.4~18 GHz) with thicknesses of 4.6 mm. The excellent low-frequency absorption performance proved that the CMF/FeNi-SiO_2 magnetic and insulating double-layer structure composites outperformed the other absorbers. Table 1 shows the microwave absorption properties of several recently published typical composites formed by carbon foam, magnetic alloy and SiO_2. By comparison, the modified carbon foam we obtained had the unique advantages of greater reflection loss values and better low-frequency microwave absorption capacities.

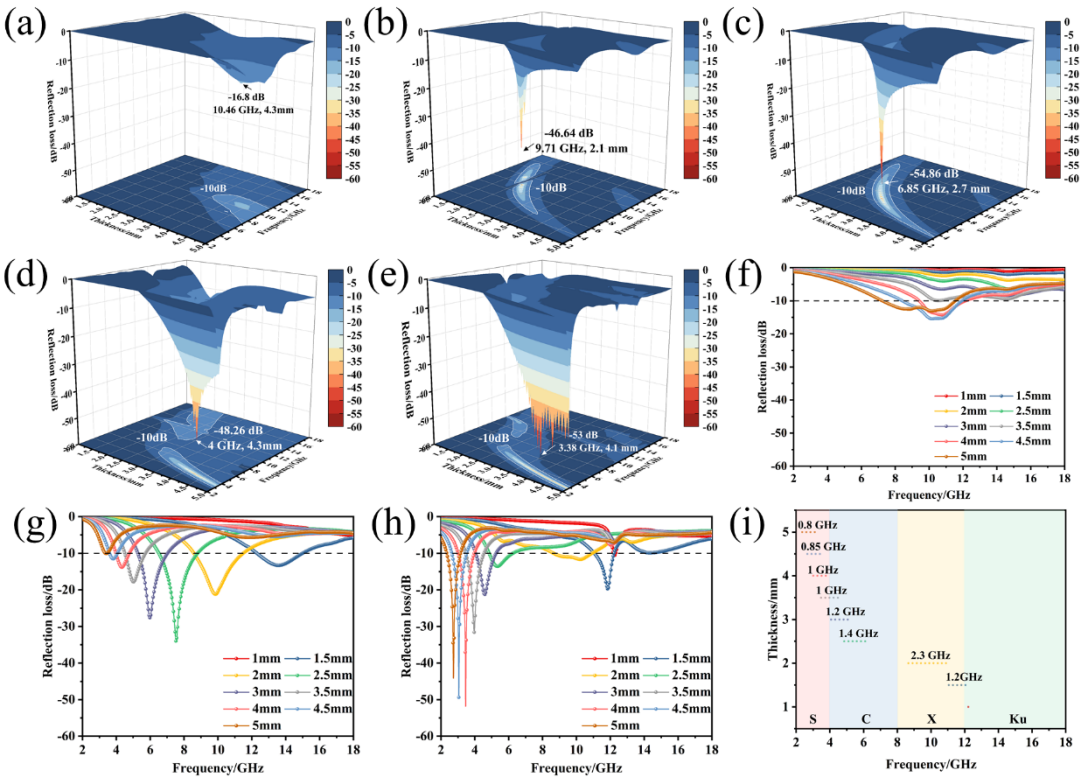

Figure 6 The 3D RL maps of CMF-based absorbers of d at 1~5 mm in 2~18 GHz, (a) CMF, (b) CMF/FeNi10, (c) CMF/FeNi15, (d) CMF/FeNi10-SiO_2, (e) CMF/FeNi15-SiO_2, (f) ~ (h) RL curves of CMF, CMF/FeNi15 and CMF/FeNi15-SiO_2 samples, respectively, (i) effective absorption range of CMF/FeNi15-SiO_2 at different

layer thicknesses.

Table 1 Microwave absorption properties of carbon materials and magnetic alloy, SiO_2 composites published in recent years.

Materials	Matching thickness (mm)	RL value (dB)	Frequency (GHz)	Bindwidth(GHz) (RL < -10 dB)	Ref.
CoNi@PRM-NC	1.7	-56	17.8	6.1 ~ 18	[11]
CuNi/CF	1.7	-50.2	15.92	3 ~18	[12]
CoFe@C	2.6	−73.63	11.6	9 ~ 18	[32]
C /$CoFe_2O_4$/(Fe,Ni)	2.0	-34.3	12.92	3.8 ~ 18	[33]
CoNi/NG hybrids	2	-22	10	3.6-18	[46]
$FeNi_3$@SiO_2@rGO–PANI	2.4	-40.18	14	10.08 ~ 10.8 12.08 ~ 18	[35]
CF/FeCo-SiO_2	5	−43.78	4.64	4.08 ~ 18	[39]
Fe@SiO_2 NCs	2.81	−61.6	9	6 ~ 18	[47]
Fe_3O_4/SiO_2/graphene	1.5	−27.1	12.2	3.3 ~ 13.6	[48]
CMF/FeNi15	2.7	-54.86	6.85	3.3 ~ 15.3	This work
CMF/FeNi15-SiO_2	4.1	-53	3.38	2.4 ~ 6.5 8.4 ~ 12.4	This work

To study the microwave absorption mechanism, the complex dielectric permittivity ($\varepsilon_r=\varepsilon' - j\varepsilon''$) and magnetic permeability ($\mu_r=\mu' - j\mu''$) of the CMF-based foams were measured and shown in Figure 7. In Figure 7(a), the ε' of CMF was stable in the whole frequency with the value of 3. After the FeNi alloy was decorated on the CMF surface, the ε' was greatly improved to 13 and 15.5 for CMF/FeNi10 and CMF/FeNi15 at 2 GHz, respectively, which decreased slightly to the value of 10 at 18 GHz. When coating SiO_2 layer onto the FeNi film, the ε' showed a declined trend with the sequence of ε'(CMF/FeNi15) > ε'(CMF/FeNi10) > ε'(CMF/FeNi15-SiO_2) > ε'(CMF/FeNi10-SiO_2). Meanwhile, the ε'' showed an upward trend in the whole frequency for CMF/FeNi composites and the value of ε'' reached 10.5 at 18 GHz, while the ε'' of CMF was in the range of 0.5~3.8 GHz, indicating enhanced storage

and dissipation capabilities. In addition, the ε″-f curves for the CMF/FeNi15-SiO_2 double-layer structure showed one resonance peak at 7 GHz, which was caused by the interfacial polarization associated with the presence of CMF, FeNi and SiO_2. The $\tan\delta_\varepsilon$ value of CMF/FeNi10-SiO_2 was the highest among the five samples in the 2~18 GHz, as shown in Figure 7(c), proving that double-layers structure could improve the dielectric loss abilities significantly.

Figure 7(d) showed that the μ′ of the CMF/FeNi10 and CMF/FeNi15 declined with the frequency. But there was an obvious peak at 12 GHz for CMF/FeNi10-SiO_2 and CMF/FeNi15-SiO_2 which was related to exchange resonance[49]. Another possible reason may be from the coupling effect of the interface between SiO2 and FeNi. Coating diamagnetic layer on a magnetic material can cause such a coupling effect that had also reported by other paper [50]. Furthermore, such a coupling effect also affects the frequency response of others peaks in μ″. As indicated in the Figure 7(e), we can find the shifts of two peaks: before coating the position of them were at 14-18 GHz; while after coating, both of them shifted to lower frequency, 6-10 GHz. Thus the appearance of the peak at 12 GHz would be related with the coupling effect. Figure 7(f) showed magnetic loss tangents ($\tan\delta_m$) of the complex permeability for CMF and CMF-based absorbers, the $\tan\delta_m$ values of CMF/FeNi10 and CMF/FeNi15 approximated that of CMF, while the $\tan\delta_m$ value of CMF/FeNi15-SiO_2 structure was the highest among the five absorbers, indicating its significant magnetic loss

capability.

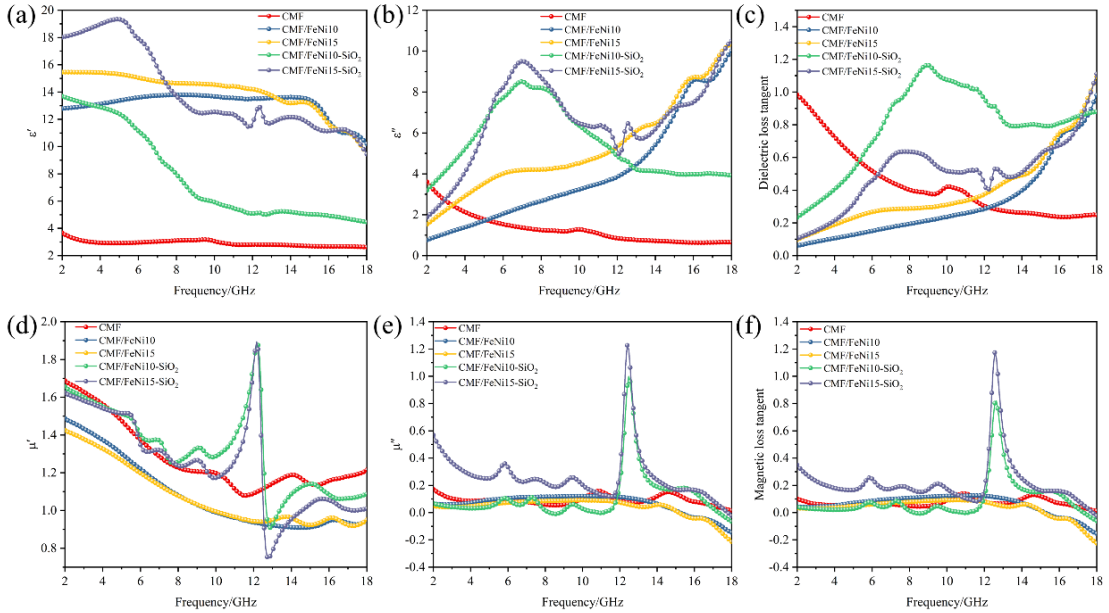

Figure 7 (a) Real and (b) imaginary part of the permittivity, (c) dielectric loss tangent, (d) real and (e) imaginary part of the permeability, (f) magnetic loss tangent of the samples.

Generally, there are two main factors affecting microwave absorption, namely impedance matching and attenuation characteristics. When the impedance of the absorber Z_{in} is expected to be equal to the characteristic impedance of the air Z_0, impedance matching can allow more microwaves to enter the absorber and reduce reflections from the absorber surface. The impedance matching ratio ($Z = Z_{in} / Z_0$) of the samples were shown in Figure 8. As shown in Figure 8(a), the Z value of CMF was far away from 1 with the thickness range of 1~5mm, resulting in poor impedance matching, which delineated the poor microwave absorbing performance in the whole frequency range. When FeNi was deposited on CMF, the Z values of CMF/FeN10 and CMF/FeN15 were close to 1 from 6 to 12 GHz, proving the excellent microwave absorption performance in the X band. However, the impedance matching of CMF/FeN10 and CMF/FeN15 was far away from 1 in the frequency range of 2~6

GHz, leading to poor absorption properties in the low-frequency band. Interestingly, when SiO_2 was coated on FeNi film, the impedance matching of CMF/FeN10-SiO_2 and CMF/FeN15-SiO_2 were nearly to 1 in S and C bands, which meant more microwaves could easily enter the absorber, thus improving the microwave absorption capabilities of S and C bands.

The attenuation constant (α) was introduced to evaluate the microwave absorption

performance and can be calculated by the following expression. Usually, the higher the attenuation constant, the more waves can be attenuated in the absorber.

$$\alpha = \frac{\sqrt{2}\Pi f}{c} \times \sqrt{\left(\mu'' \varepsilon'' - \mu' \varepsilon'\right) + \sqrt{\left(\mu'' \varepsilon'' - \mu' \varepsilon'\right)^2 + \left(\mu'' \varepsilon' + \mu' \varepsilon''\right)^2}} \quad (4)$$

Figure 8(f) showed the frequency-dependent attenuation constant of the samples. Among the five samples, CMF had the smallest α value and remained stable with frequency. For FeNi coated CMF, the α was greatly improved to the value of 450 at 18 GHz. While for FeNi-SiO_2 double-layer coated CMF, the α was further enhanced over the whole frequency range, which implied that the magnetic-insulating dual-layer structure can enormously enhance the attenuation abilities.

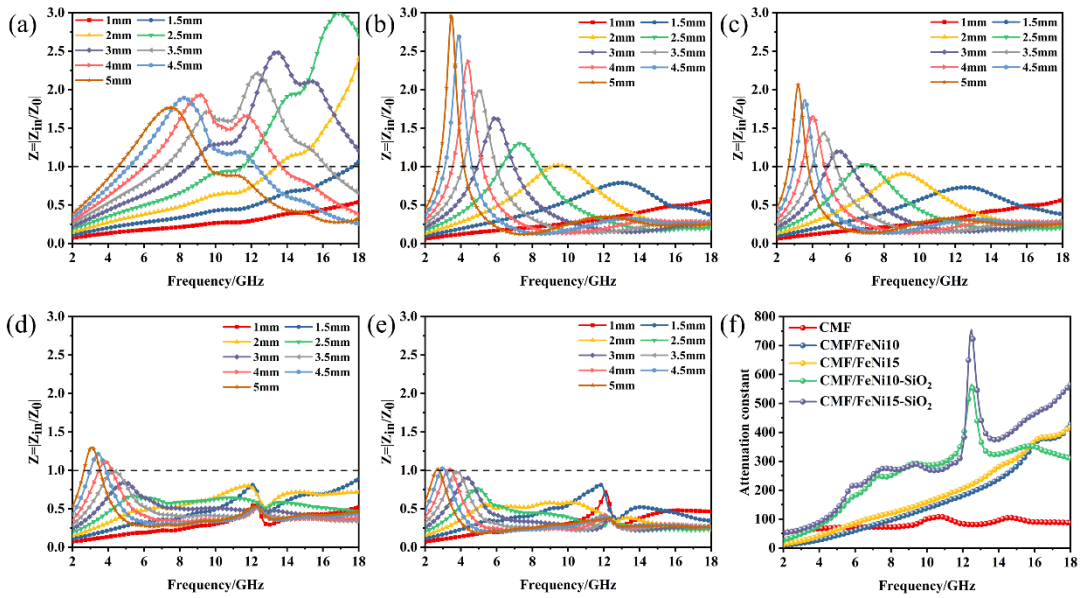

Figure 8 Calculated Z values versus frequency curves of (a) CMF, (b) CMF/FeNi10, (c) CMF/FeNi15, (d) CMF/FeNi10-SiO_2, (e) CMF/FeNi15-SiO_2 and (f) Attenuation constants versus frequency curves

To further study the attenuation mechanism of microwave absorption performance, the dielectric loss and magnetic loss were also studied in detail. As a whole, the magnetic losses of samples may be affected by natural ferromagnetic resonance, exchange resonances and eddy current loss. Eddy current loss was evaluated by the value $C_0 = \mu''(\mu')^{-2}f^{-1}$. If the values of C_0 kept constant over the frequency range, it meant that the magnetic loss entirely relied on eddy current loss [27]. As shown in Figure 9(a), the C_0 values of the CMF/FeNi were stable in 4~12 GHz, proving that the eddy current loss was the main mechanism of magnetic loss. The C_0 ~ f curves of CMF/FeNi15-SiO_2 drastically fluctuated over the whole frequency. The peaks located at 9.5 GHz and 13 GHz were attributed to the exchange resonance, which usually happened in the high-frequency band. Compared with the μ''- f curves in Figure 7(e), the peaks at 6 GHz and 7 GHz may be caused by natural resonance. Thus, in addition to the eddy current losses, exchange resonance and

natural resonance also contributed to the magnetic loss that affected the absorption performance.

Dielectric loss is another indispensable microwave absorption mechanism. It is evaluated by Debye's relaxation theory:

$$\left(\varepsilon_r^{'} - \varepsilon_{r\infty}\right)^2 + \left(\varepsilon_r^{''}\right)^2 = \left(\varepsilon_r^{'} - \varepsilon_{r\infty}\right)(\varepsilon_{r0} - \varepsilon_{\infty}) \quad (5)$$

This equation represents a Cole-Cole semicircle with the center on the ε_r' axis, a semicircle indicating a Debye relaxation process has occurred in the material. Figure 9(b) showed three distinct Cole-Cole semicircles for CMF that indicated the Debye relaxation losses in the CMF. While after deposition of SiO_2, as shown in Figure 9(e) and (f), there were more cole-cole semicircles than that of CMF, indicating that more relaxations existed in the CMF/FeNi-SiO_2, such as interfacial polarization.

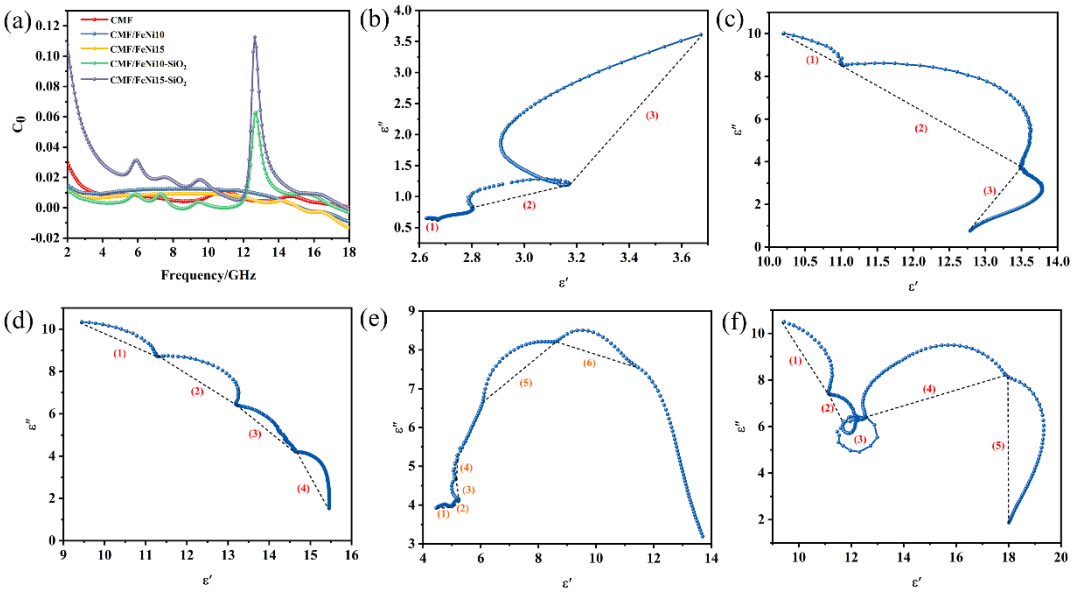

Figure 9 (a) curves of C_0 vs f, (b)~(f) Typical ε″- ε′ curves of CMF and CMF/FeNi10, CMF/FeNi15, CMF/FeNi10-SiO_2, CMF/FeNi15-SiO_2.

Additionally, to explain the EMW absorption characteristics, the quarter wavelength matching model was used in the discussion:

$$d_m = \frac{n\lambda}{4} = \frac{nc}{4f_m\sqrt{|\mu_r||\varepsilon_r|}} (n = 1, 3, 5, \ldots) \quad (6)$$

where λ_m is the wavelength, $|\mu_r|$ and $|\varepsilon_r|$ are the modulus of complex permeability and permittivity, respectively. According to equation (6), when the thickness of the absorber is equal to λ/ 4, the phase difference between the two reflected waves reflected from the air-absorber and absorber-metal interface is 180 °, which offsets each other. Figure 10 (a) and (b) showed the relationship between f_m and d_m of CMF/FeNi15 and CMF/FeNi15-SiO_2. Clearly, with the increase in thickness, the RL_{min} matching frequency shifted to the low band. Figure 10 showed that the experimental d_m was almost located in the λ / 4 curve, showing that the better microwave absorption performance of CMF/FeNi15 and CMF/FeNi15-SiO_2 than pure CMF could be explained by the quarter wavelength theory.

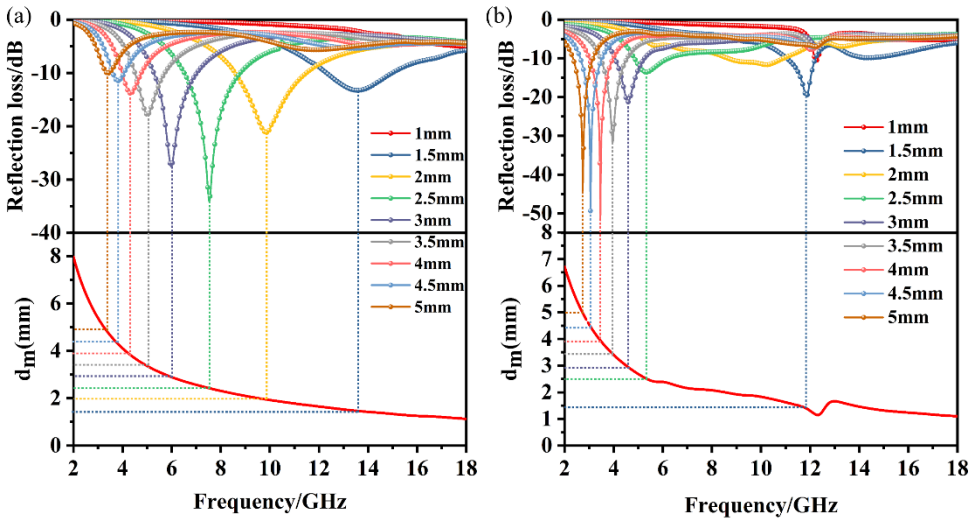

Figure 10 RL curves and dependence of the absorber matching thickness (d_m) versus matching frequency (f_m) under wavelengths of λ/4 model for (a) CMF/FeNi15 and (b) CMF/FeNi15-SiO_2.

Based on the results above, the electrowave absorption mechanism of FeNi-SiO_2 can be concluded in Figure 11. Firstly, the three-dimensional porous structure of carbon foam can reflect electrowave multiple times to attenuate the electrowave energy.

Secondly, the good conductivity of carbon foam and FeNi alloy can cause conductivity loss to transfer electrowave energy into energy. Then, due to the different electronegativity between carbon and FeNi alloy, FeNi alloy and SiO_2, the electromagnetic field at their interface will cause interface scattering and polarization, which enhanced dielectric loss. Finally, the outermost layer of the SiO_2 insulating layer can adjust magnetic loss and dielectric loss that leading to higher attenuation capabilities and better impedance matching, especially at the low-frequency band, ultimately improving microwave absorption capability. In short, the as-prepared CMF/FeNi-SiO_2 is a promising electromagnetic absorbing material.

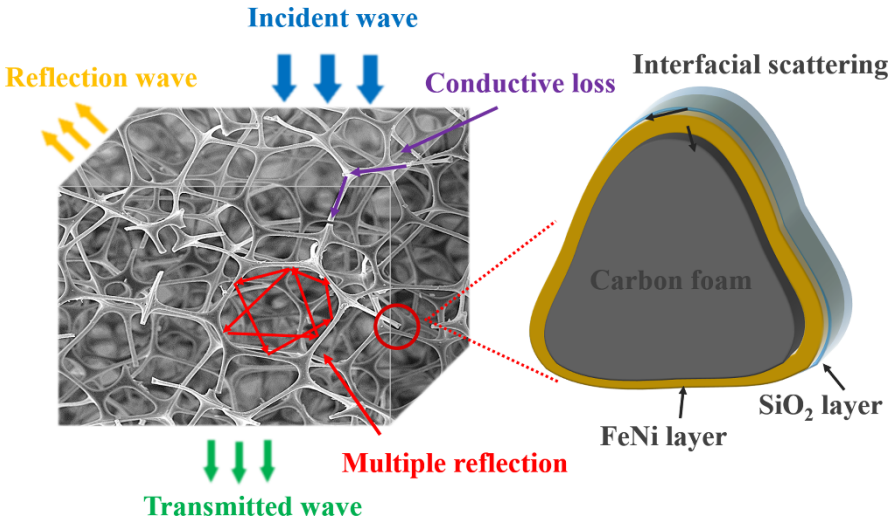

Figure 11 Schematic illustration of microwave absorption mechanisms in CMF/FeNi-SiO_2.

4. Conclusion

The porous carbonated melamine foam (CMF) double-coated by the FeNi alloy and SiO_2 layer (CMF/FeNi-SiO_2) with excellent performant microwave absorption was prepared using magnetron sputtering method. By varying the sputtering time, the content of FeNi and SiO_2 layers could be modulated. The as-prepared CMF/FeNi15 had the RL_{min} of -54.86 dB at 6.85 GHz and the EAB was 2.06 GHz (from 5.94 GHz to 8 GHz) with a thickness of 2.7 mm. The CMF/FeNi15-SiO_2 exhibited an RL_{min} of

−53 dB at 3.38 GHz and an EAB of 0.93 GHz covering 2.93 ~ 3.86 GHz at 4.1 mm. The frequency bandwidth of 4 GHz (2.35~6.35 GHz) with absorption loss ≤ −10 dB and the frequency bandwidth of 2.05 GHz (2.62~4.67 GHz) with absorption loss ≤ -20 dB demonstrated the CMF/FeNi15-SiO_2 a high-efficient absorber in the low-frequency band (2-6 GHz). The excellent electrowave absorption properties in the low-frequency band were due to the multiple reflections of the three-dimensional structure, the conductive loss caused by the carbon skeleton, the high attenuation ability of the FeNi alloy and the good impedance of SiO_2. This high microwave absorption performance has provided a high potential for the porous carbon foam modified by magnetic metal and SiO_2 in the use of anti-electromagnetic pollution.

Declaration of Competing Interest

The authors declare that they have no known competing financial interests or personal relationships that could have appeared to influence the work reported in this paper.

Acknowledgment

This work is supported by the National Natural Science Foundation of China (Grant No. 52002403), the key project of Changsha (Grant No kh2103011) and the China Hunan Provincial Science& Technology Department (Grant No 2020GK2051).

References

1. Wu, N., et al., *Review on the electromagnetic interference shielding properties of carbon based materials and their novel composites: Recent progress, challenges and prospects.* Carbon, 2021. **176**: p. 88-105.
2. Liu, J., et al., *Hydrophobic, Flexible, and Lightweight MXene Foams for High-Performance Electromagnetic-Interference Shielding.* Advanced Materials, 2017. **29**(38).
3. Zhang, Y., et al., *Broadband and Tunable High-Performance Microwave Absorption of an Ultralight and Highly Compressible Graphene Foam.* Advanced Materials, 2015. **27**(12): p. 2049-2053.
4. Song, Q., et al., *Graphene and MXene Nanomaterials: Toward High‐Performance Electromagnetic Wave Absorption in Gigahertz Band Range.* Advanced Functional Materials, 2020. **30**(31).
5. Gupta, S. and N.-H. Tai, *Carbon materials and their composites for electromagnetic interference shielding effectiveness in X-band.* Carbon, 2019. **152**: p. 159-187.
6. Kumar, R., et al., *Recent progress on carbon-based composite materials for microwave electromagnetic interference shielding.* Carbon, 2021. **177**: p. 304-331.

7. Qu, B., et al., *Coupling Hollow Fe3O4-Fe Nanoparticles with Graphene Sheets for High-Performance Electromagnetic Wave Absorbing Material.* Acs Applied Materials & Interfaces, 2016. **8**(6): p. 3730-3735.
8. Ren, Y.L., et al., *Quaternary Nanocomposites Consisting of Graphene, Fe3O4@Fe Core@Shell, and ZnO Nanoparticles: Synthesis and Excellent Electromagnetic Absorption Properties.* Acs Applied Materials & Interfaces, 2012. **4**(12): p. 6436-6442.
9. Sun, D.P., et al., *Controlled synthesis of porous Fe3O4-decorated graphene with extraordinary electromagnetic wave absorption properties.* Acta Materialia, 2013. **61**(15): p. 5829-5834.
10. Zhao, S.C., et al., *Alternate nonmagnetic and magnetic multilayer nanofilms deposited on carbon nanocoils by atomic layer deposition to tune microwave absorption property.* Carbon, 2016. **98**: p. 196-203.
11. Yan, J., et al., *The 3D CoNi alloy particles embedded in N-doped porous carbon foams for high-performance microwave absorbers.* Carbon, 2019. **152**: p. 545-555.
12. Lyu, L., et al., *CuNi alloy/ carbon foam nanohybrids as high-performance electromagnetic wave absorbers.* Carbon, 2021. **172**: p. 488-496.
13. Liu, Q.H., et al., *CoNi@SiO2@TiO2 and CoNi@Air@TiO2 Microspheres with Strong Wideband Microwave Absorption.* Advanced Materials, 2016. **28**(3): p. 486-490.
14. Chen, Q., et al., *Polymer-Derived Lightweight SiBCN Ceramic Nanofibers with High Microwave Absorption Performance.* ACS Appl Mater Interfaces, 2021. **13**(29): p. 34889-34898.
15. Mao, B., et al., *Synthesis and microwave absorption properties of multilayer SiC/C foam with alternating distribution of C and SiC.* Journal of Alloys and Compounds, 2021. **879**.
16. Jiang, Y., et al., *Lightweight spongy bone-like graphene@SiC aerogel composites for high-performance microwave absorption.* Chemical Engineering Journal, 2018. **337**: p. 522-531.
17. Ye, F., et al., *Direct Growth of Edge-Rich Graphene with Tunable Dielectric Properties in Porous Si3N4 Ceramic for Broadband High-Performance Microwave Absorption.* Advanced Functional Materials, 2018. **28**(17).
18. Kruzelak, J., et al., *Progress in polymers and polymer composites used as efficient materials for EMI shielding.* Nanoscale Advances, 2021. **3**(1): p. 123-172.
19. Bradford, P.D., et al., *Tuning the compressive mechanical properties of carbon nanotube foam.* Carbon, 2011. **49**(8): p. 2834-2841.
20. Hu, K., et al., *Ultralight Ti3C2Tx MXene foam with superior microwave absorption performance.* Chemical Engineering Journal, 2021. **408**.
21. Shahzad, F., et al., *Electromagnetic interference shielding with 2D transition metal carbides (MXenes).* Science, 2016. **353**(6304): p. 1137-1140.
22. Inagaki, M., J.S. Qiu, and Q.G. Guo, *Carbon foam: Preparation and application.* Carbon, 2015. **87**: p. 128-152.
23. Moglie, F., et al., *Electromagnetic shielding performance of carbon foams.* Carbon, 2012. **50**(5): p. 1972-1980.
24. Chen, Y., et al., *Highly Sensitive, Flexible, Stable, and Hydrophobic Biofoam Based on Wheat Flour for Multifunctional Sensor and Adjustable EMI Shielding Applications.* ACS Appl Mater Interfaces, 2021. **13**(25): p. 30020-30029.
25. Liu, P.B., et al., *Synthesis of lightweight N-doped graphene foams with open reticular structure for high-efficiency electromagnetic wave absorption.* Chemical Engineering Journal, 2019. **368**: p. 285-298.
26. Gupta, S. and N.-H. Tai, *Carbon materials as oil sorbents: a review on the synthesis and performance.* Journal of Materials Chemistry A, 2016. **4**(5): p. 1550-1565.
27. Feng, W., M. Qin, and Y. Feng, *Toward highly thermally conductive all-carbon composites: Structure control.* Carbon, 2016. **109**: p. 575-597.
28. Ye, X., et al., *Synthesis and microwave absorption properties of novel reticulation SiC/Porous melamine-derived carbon foam.* Journal of Alloys and Compounds, 2019. **791**: p. 883-891.
29. Liu, H., et al., *Carbon foams: 3D porous carbon materials holding immense potential.* Journal of Materials Chemistry A, 2020. **8**(45): p. 23699-23723.
30. Li, Y., et al., *3D hierarchical Co3O4/Reduced graphene oxide/melamine derived*

carbon foam as a comprehensive microwave absorbing material. Journal of Alloys and Compounds, 2019. **792**: p. 424-431.
31. Qiu, Y., et al., *MOFs derived flower-like nickel and carbon composites with controllable structure toward efficient microwave absorption.* Composites Part A: Applied Science and Manufacturing, 2022. **154**.
32. Qiu, Y., et al., *Structure design of Prussian blue analogue derived CoFe@C composite with tunable microwave absorption performance.* Applied Surface Science, 2022. **571**.
33. Yin, P., et al., *Structure regulation in N-doping biconical carbon frame decorated with CoFe2O4 and (Fe,Ni) for broadband microwave absorption.* Chemical Engineering Journal, 2022. **446**.
34. Liu, H., et al., *Preparation and the electromagnetic interference shielding in the X-band of carbon foams with Ni-Zn ferrite additive.* Journal of the European Ceramic Society, 2016. **36**(16): p. 3939-3946.
35. Ding, X., et al., *Excellent electromagnetic wave absorption property of quaternary composites consisting of reduced graphene oxide, polyaniline and FeNi3@SiO2 nanoparticles.* Applied Surface Science, 2015. **357**: p. 908-914.
36. Mazur, M., et al., *Functional photocatalytically active and scratch resistant antireflective coating based on TiO 2 and SiO 2.* Applied Surface Science, 2016. **380**: p. 165-171.
37. Fleaca, C.T., et al., *Novel Fe@C–TiO2 and Fe@C–SiO2 water-dispersible magnetic nanocomposites.* Applied Surface Science, 2013. **278**: p. 284-288.
38. Shen, Y., et al., *Ni/NiO/SiO2/C nanofibers with strong wideband microwave absorption and robust hydrophobicity.* Applied Surface Science, 2022. **588**.
39. Wei, Y., et al., *Enhanced magnetic and microwave absorption properties of FeCo-SiO2 nanogranular film functionalized carbon fibers fabricated with the radio frequency magnetron method.* Applied Surface Science, 2018. **428**: p. 296-303.
40. Pan, Y., et al., *Inorganic/organic bilayer of silica/acrylic polyurethane decorating FeSiAl for enhanced anti-corrosive microwave absorption.* Applied Surface Science, 2021. **567**.
41. Green, M., et al., *Doped, conductive SiO2 nanoparticles for large microwave absorption.* Light-Science & Applications, 2018. **7**.
42. Guo, R., et al., *Core-rim structured carbide MXene/SiO2 nanoplates as an ultrathin microwave absorber.* Carbon, 2020. **169**: p. 214-224.
43. Wang, J., et al., *Hierarchical Carbon Fiber@MXene@MoS2 Core‐sheath Synergistic Microstructure for Tunable and Efficient Microwave Absorption.* Advanced Functional Materials, 2020. **30**(45).
44. Biesinger, M.C., et al., *Resolving surface chemical states in XPS analysis of first row transition metals, oxides and hydroxides: Sc, Ti, V, Cu and Zn.* Applied Surface Science, 2010. **257**(3): p. 887-898.
45. Tian, W., et al., *Atomic-Scale Layer-by-Layer Deposition of FeSiAl@ZnO@Al2O3 Hybrid with Threshold Anti-Corrosion and Ultra-High Microwave Absorption Properties in Low-Frequency Bands.* Nanomicro Lett, 2021. **13**(1): p. 161.
46. Feng, J., et al., *Interfacial interactions and synergistic effect of CoNi nanocrystals and nitrogen-doped graphene in a composite microwave absorber.* Carbon, 2016. **104**: p. 214-225.
47. Javid, M., et al., *Strong microwave absorption of Fe@SiO2 nanocapsules fabricated by one-step high energy plasma.* Journal of Physics and Chemistry of Solids, 2019. **129**: p. 242-251.
48. Liu, X.F., et al., *Graphene-enhanced microwave absorption properties of Fe3O4/SiO2 nanorods.* Composites Part a-Applied Science and Manufacturing, 2016. **89**: p. 40-46.
49. Cheng, Y., et al., *A Flexible and Lightweight Biomass-Reinforced Microwave Absorber.* Nanomicro Lett, 2020. **12**(1): p. 125.
50. Wang, Y., et al., *Carbon supported MnO2-CoFe2O4 with enhanced electrocatalytic activity for oxygen reduction and oxygen evolution.* Applied Surface Science, 2017. **403**: p. 51-56.